THz-Photoconductivity and THz-Conductivity in Metal-Organic Frameworks (MOFs)

Jens Neu, Sarah Ostresh, Brian Pattengale, and Gary W. Brudvig Yale University, New Haven, CT, 06511 USA

Abstract—Metal-organic frameworks are a class of emerging materials, with novel, designable, and outstanding properties. Terahertz (THz) spectroscopy is a versatile technique to explore low-energy resonant modes in these materials, and conductivity and photoconductivity. Understanding mechanism and timescales of photoconductivity in metal-organic frameworks (MOFs) is crucial for their applicability in solar energy generation. The subps time resolution of optical pump-THz probe (OPTP) in combination with time-resolved THz spectroscopy (TRTS) provides an unmatched view into the life of a photoelectron within MOFs. In this talk, I will present our experiments studying conductivity and photoconductivity in two MOFs, namely di-Zn(II)-tetrathiafulvalene-tetrabenzoate (Zn₂TTFTB) and di-Mn(II)-2,5-dimercaptoterephthalate (Mn₂DSBDC).

I. INTRODUCTION

THz time domain spectroscopy (TDS) [1], optical pump-THz probe (OPTP), and time-resolved THz spectroscopy (TRTS) have been extensively employed to understand conductivity and photoconductivity in semiconducting materials, starting in the 1990's with measurements on silicon [2]. THz spectroscopy became an increasingly recognized and appreciated technique to explore conductivity and photoconductivity. Its applications have been expended to explore conductivity, phonons, and polaritons in perovskites [3], 2D carbides and nitrides, and other 2D materials [4]. In the last three years, these outstanding techniques have also been utilized to understand metal-organic frameworks (MOFs) better

Air stable MOFs were first synthesized 1999 [5]. In the 23 years since their discovery, the number of publications on MOFs have been rapidly growing; currently about 10% of the structures in the Cambridge Crystallographic Database are MOFs. This growth is motivated by their outstanding properties, and the easiness to modify and design MOFs. MOFs are formed by organic linkers that coordinate metal centers in either a 3D, 2D, or 1D configuration. This approach is rather flexible and replacing linkers can be used to tailor the properties of a MOF. For example, aromatic linkers, such as tetrathiafulvalenetetrabenzoate (TTFTB⁴⁻), can be incorporated into a MOF to provide a well-defined visible absorption.

The framework formed by these linkers commonly exhibits large pores and cavities (see Fig. 1 b). The porosity provides an additional incentive to study MOFs, e.g. for gas storage, catalysis, and ultralight devices. These promising applications in combination with the ease of synthesis and modification gave rise to the huge number of novel MOFs, reaching more than a hundred thousand published structures.

While the field of MOFs is rapidly growing, THz research within this field is still underrepresented. However, in the last few years several groups have endeavored into this new frontier and my talk will highlight two of our recent publications in the novel and emerging field of conductive MOFs.

THz spectroscopy of conductive MOFs is particularly rewarding because, in contrast to DC techniques, THz does not require complicated electrode fabrication and avoids introducing contact resistance that clouds the reliability of the measured conductivity. Furthermore, the short range of THz measurements allows us to separate inter- and intra-particle conductivity providing an unmatched view into the conductivity of these novel materials.

In this talk, I will present THz TDS on Zn₂TTFTB and di-Mn(II)-2,5-dimercaptoterephthalate (Mn₂DSBDC), as well as OPTP and TRTS measurements of the photoconductive MOF Zn₂TTFTB [6,7].

II. MATERIALS

As this presentation is focused on THz spectroscopy, I refer to our previous publications for most of the fabrication details [6,7], as well as the publications which first reported the synthesis of these MOFs [8,9].

In addition to synthesizing these MOFs, we also performed metal exchanges in Mn_2DSBDC . The MOF was dissolved in DMF (an organic solvent) and mixed with an organic copper, cobalt, or nickel salt. This mixture was held at $100^{\circ}C$ for 21 h, after which the product was filtered out. Following synthesis and metal exchange, we measured powder X-ray diffraction (PXRD) patterns to confirm the structural identity with previously published structures, shown in Figure 1 [6-9].

This rather simple technique revealed that the metal exchange was successful, meaning the lattice of the resulting MOF was very similar to the original lattice. As shown in the PXRD pattern in Fig. 1c and d, the exchange did not destroy the original pattern, but merely shifted some of the peaks by 0.1 degree. This minute shift is indicative of a decrease in spacing, and proof of successful incorporation of the guest molecules.

III. TDS, OTPT, AND TRTS ON ZN2TTFTB

Zn₂TTFTB is a 3D semiconducting MOF formed by zinc nodes connected by TTFTB⁴⁻ linkers. This MOF has a broad absorption from 700 nm down to below 300 nm. This broad absorption provides an excellent overlap with the solar spectrum making this material particularly interesting for light harvesting applications. In order to understand the photophysics in this material, we measured OPTP and TRTS under 400 nm light excitation. Additionally, we also collected TDS spectra and processed these to gain the complex static refractive index of this MOF.

In order to understand the as-synthesized materials and avoid any unintended modification, we assembled the MOF powder into a simple tape cell. This cell is built by punching a hole into a business card (or mylar sheet) with known thickness. The bottom of this hole is sealed with a piece of regular scotch tape,

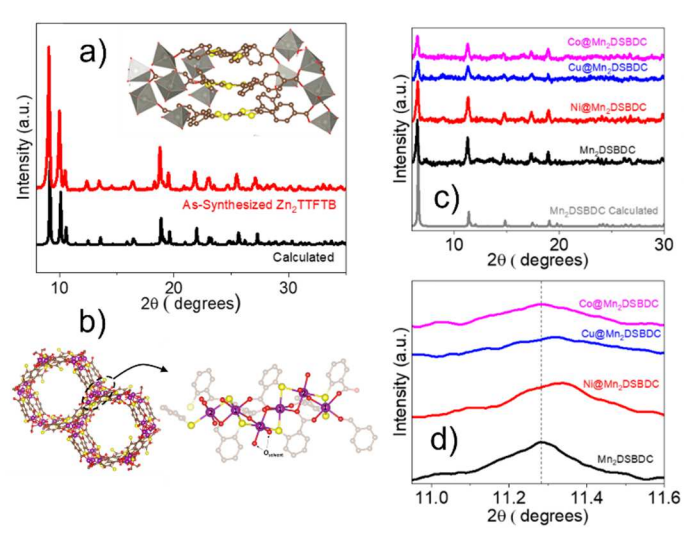


Fig. 1. a) Powder X-ray diffraction (PXRD) pattern of Zn₂TTFTB as synthesized (red) compared to the spectrum calculated from the previously published structure (black). Inset illustrates the building blocks of this MOF in a simplified manner. b) structure of Mn₂DSBDC. The two different manganese centers (purple) are labeled with 1 and 2. c) PXRD of Mn₂DSBDC (black) compared to the calculated spectrum (gray). The inclusion of Ni, Cu, and Co did not destroy the structure as can be seen be the decent agreement between the patterns. However, the zoom in view (d)) shows a contraction of the unit cell upon metal exchange. Reprint from [6,7].

which is THz transparent. The single side sealed hole is then filled with the MOF powder and this powder is enclosed using a second piece of tape. This sample preparation yields an ill-defined mixture of sample powder and air and as such the results gained from these measurements, in particular the accurate magnitude, ought to be taken with a grain of salt. But this preparation avoids pressure, heat, solvents, and other commonly needed external stresses in sample fabrication. As such, this method yields the closest to as-synthesized sample as possible.

While the accurate magnitude of the refractive index might need scaling to account for the air-sample mixture, resonant modes will not be influenced by this sample preparation. To emphasize the advantage of this sample preparation, we compared the absorption coefficient for two samples in Fig 2a and 2b. Both samples were prepared from the same material stock. The only difference was that for the second sample pressure of 11 kbar was applied before the measurement. The application of pressure would be needed to press Teflon pellets and can be avoided when building a tape-cell.

We measured the THz transmission through both sample cells, shown in Fig. 2. The pristine cell (a) shows a three rather equally strong resonances at 0.5, 0.71, and 0.95 THz. In contrast, the same material after applying pressure (b) shows two resonances, at 0.5 and 0.8 THz. The pressure dependence of the modes was first observed when assembling cells and accidently pressing the cell with a bare human thumb. Higher pressure resulted in a more pronounced difference. While the difference in the THz mode is clearly visible and striking, the PXRD pattern of the MOF did not change. We concluded that the main effect of pressure in this MOF was the expelling of inclusion molecules, most-likely DMF molecules, captured in the MOF pores during synthesis. This result underlines that THz can provide information complementing more common PXRD techniques. This is particularly important for MOFs in

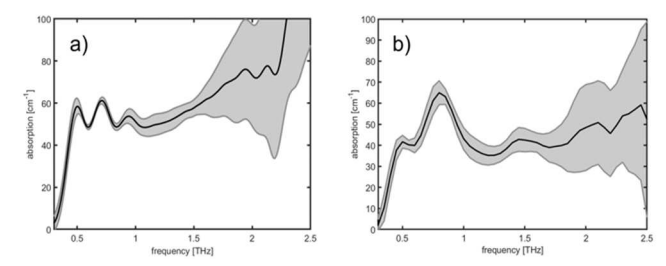


Fig. 2. Absorption coefficient of Zn₂TTFTB a) in its pristine form and b) after application of 11 kbar pressure. The pressure was not applied during the measurement but solely during the sample preparation step. The pressure clearly altered the relative magnitude of the absorption modes. PXRD (not shown) did not reveal a structural change; hence, we concluded that the THz modes were sensitive to guest molecules (most-likely DMF) that were squeezed out of the sample by the external pressure.

which guest molecule inclusions and gas capturing can massively change electro-optical properties while being undetectable in PXRD.

Following the TDS measurements, we collected OPTP traces of the same material, shown in Fig. 3a. We measured an instrument response limited onset of photoconductivity as well

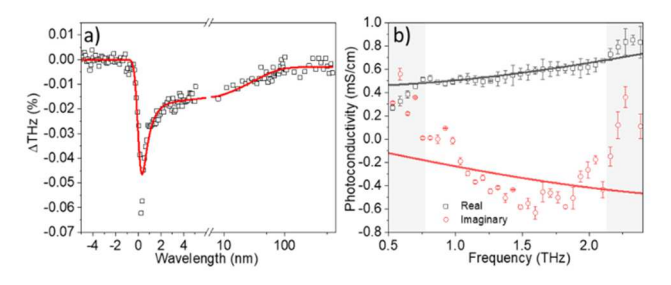


Fig. 3. THz photoconductivity of Zn_2TTFTB under 400 nm excitation. a) The OPTP measurements show an ultrafast onset of photoconductivity within the instrument response limits. The decay follows three distinguishable time scales, one being instrument response limited, the second on the 30 ps time scale and finally a long time offset. For clarity, the first 6 ps are plotted on a linear scale and the remaining time is plotted on a logarithmic scale. b) TRTS measured 200 fs after photoexcitation. This time frame was selected to provide sufficient signal to noise while avoiding non-linear pump-probe interactions. The solid lines show the Drude-Smith fit on the collected TRTS spectra.

as an ultrafast decay. In addition to these very fast photoinduced properties, we also clearly detect a slower component as well as a long time offset (please note the semi-log time scale of the plot). The OPTP results are fitted with a three-component exponential function with amplitudes A_i and decay times τ_i , convoluted with the instrument response function of width τ_0 :

$$\Delta THz = \left[\sum_{i=1}^{3} A_i exp\left(-\frac{t_{pump} - t_0}{\tau_i} \right) \right] \otimes IRF(\tau_0)$$

Four samples were globally fitted which yielded lifetimes of $\tau_1 = 0.60 \pm 0.03$ ps, $\tau_2 = 31 \pm 3$ ps, and a fixed longtime lifetime of $\tau_3 = 10$ ns. τ_3 lays outside of our spectrometer's time range and was fixed based on previous microwave photoconductivity measurements on the same material [10].

OPTP data provide an excellent and in-depth view on the carrier generation and lifetime. TRTS results complement this information with the complex photoconductivity at a given pump-probe delay. For these materials, we measured 0.2 ps after the pump-probe overlap to ensure a large enough signal to extract photoconductivity with sufficient signal to noise.

From the measured differential transmission, the complex photoconductivity is calculated. This was done without invoking the thin film approximation as the powder sample was not thin [11] and the resonances revealed by TDS could also falsify thin-film approximation results [12]. Avoiding any approximations complicates the data processing, of course, and results in lengthier numerical codes. We utilized Matlab for this task and our open-source code can be found in our recent publication [13]. This publication also provides a free software package with a graphical user interface to enable more groups to avoid potentially inaccurate approximations or just to check their results [13].

The photoconductivity plotted in Fig. 3b shows a rather small magnitude and fitted reasonably well to a Drude-Smith model: $\sigma(\omega) = \frac{\sigma_0}{1-i\omega\tau_s} \left(1 + \frac{c}{1-i\omega\tau_s}\right)$ yielding a scattering time of $\tau_s = 17 \pm 2$ fs and a c-parameter of

$$\sigma(\omega) = \frac{\sigma_0}{1 - i\omega\tau_s} \left(1 + \frac{c}{1 - i\omega\tau_s}\right)$$

 $c = -0.86 \pm 0.01$.

The c-parameter close to -1 is consistent with the microgranular sample topology that we observed in TEM images (not shown). Furthermore, these results emphasize the great advantage of TRTS compared to DC and TRMC measurements; in particular, DC measurements of this MOF powder severely underestimate the actual material conductivity because they are more a probe of the grain-to-grain charge transfer.

The presented results constitute the first OPTP/TRTS measurements on a 3D MOF [7]; however, they were published after the first OPTP measurements on any MOF performed by our colleagues in Mainz (a 2D MOF in their case) [14].

IV. TDS OF METAL-DSBDC MOFS

The second class of MOFs discussed in this presentation utilized DSBDC4- linkers to form an infinite 3D framework. In the as-synthesized version, all metal nodes were occupied by manganese [8]. This MOF was previously reported as conductive [10], easy to synthesize, and has the potential for post-synthesize modification. In our work, we replaced the original manganese centers with cobalt, copper, and nickel. These metal exchanges did not alter the structure, morphology, or crystallinity of the MOF (see Fig. 1). We employed X-ray techniques (EXAFS and XANES [6]) to understand in detail the metal exchange location and found that approximately 10% of the manganese was replaced with the guest metal. The replacement did not exhibit a side-preference (see Figure 1b) nor did it lead to formation of local clustering. As such, we treated the replacement as a structure-preserving substitution of the guest metal for Mn.

Mn₂DSBDC powder was previously measured in a two probe DC conductivity experiment [10]. The resulting conductivity was low $(2.5 \cdot 10^{-12} \text{ S/cm})$ and there are several short-comings in this type of experiments. Firstly, the electrical contacts formed between the MOF powder and electrode patches will strongly depend on surface roughness, topology, pressure, surface chemistry, and more. The resulting contact resistance will then add to the actual material resistance, which is further complicated by the grain-to-grain charge transfer within the powder which depends on the applied pressure. Bulk DCmeasurements are a very unreliable way to determine the conductivity of emerging powder materials.

shortcomings can be overcome using THz spectroscopy as a contact free probe for conductivity.

We first fabricated a tape-cell as in the previous section and measured the THz spectra of Mn₂DSBDC and the metal exchanged analogs. None of these MOFs exhibited a strong resonance in the sub 2.5 THz range in which we measured. Application of pressures of up to 15 kbar did neither alter the THz spectra nor the PXRD pattern. Encouraged by the stability of these MOFs, we prepared Teflon+MOF pellets in which the MOF sample material forms inclusions within the Teflon background matrix. The low absorption of the Teflon and the low concentration of MOFs in this 3 mm thick pellet allow us to employ simplified data processing and analysis to determine the complex refractive index from the pellet [16].

The complex refractive index is then transformed into the complex permittivity assuming negligible magnetic susceptibility $(n \approx \sqrt{\epsilon})$. With the now determined complex permittivity and the also measured properties of pure Teflon, Bruggeman and Maxwell-Garnet effective medium theory was applied to determine the complex permittivity of the MOF inclusion. This sample preparation provides superior accuracy compared to the simple tape cell but is limited to pressure-stable MOFs.

The complex permittivity is plotted in Fig. 4a, for the pure Mn-MOF at 200 K. The red solid line shows a Drude-Smith fit in permittivity [8]. The result of this fit is used to separate the static complex permittivity from the optical conductivity, which is plotted in Fig. 4b. We would like to emphasize that this assumption lumps all frequency dependent components of the permittivity into conductivity. This is a common implicit assumption invoked when reporting THz conductivity, but it

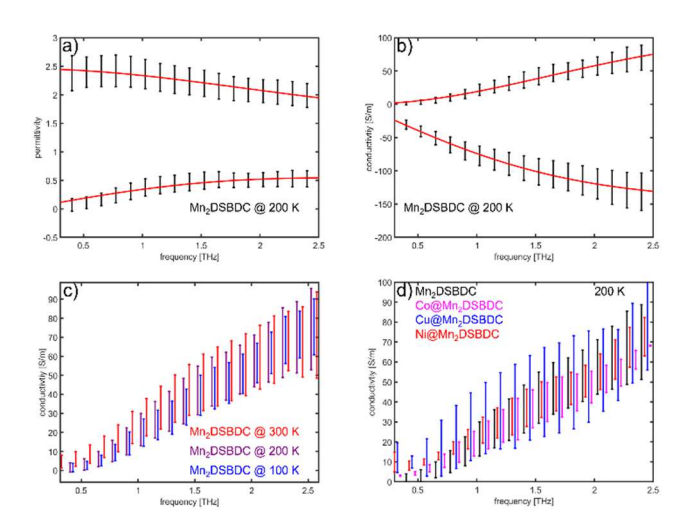


Fig. 4. THz-TDS conductivity and permittivity of Mn₂DSBDC. The sample was mixed with Teflon, pressed into pellet form, and measured in a liquid nitrogen cryostat mounted in our self-built TDS system. Effective medium theory was used to calculate the permittivity of the MOF. a) Permittivity of Mn₂DSBDC at 200 K. The red line shows the Drude-Smith fit used to separate conductivity and frequency independent permittivity. From this separation, the complex conductivity (b) was derived. c) Temperature-dependent measurements of the conductivity did not show a clear trend. d) Comparison of the conductivity of the MOFs with incorporated guest molecules. The guest molecules did not suppress the THz conductivity within this MOF. The error bars show the standard deviation from three independent samples, measured on three different locations each, resulting in nine independent measurements.

must be kept in mind when attempting to predict DC properties from THz measurements.

With a reliable method to measure the complex conductivity of this MOF family, we set out to answer two questions: firstly, does temperature influences the THz conductivity, and secondly, does the dopant metal alter THz conductivity.

Temperature-dependent measurements of the pure (and the mixed MOF) did not show a clear trend. The mean values for three spots on three Mn₂DSBDC samples are shown in Fig. 4c. There is no clear trend with temperature. At first this is puzzling as many conductivity-mechanism are thermally influenced. Commonly, thermally active dopants freeze out when the material is cooled, electron-phonon scattering is reduced, and thermally activated hopping is suppressed at lower temperatures, raising the question why the conductivity of Mn₂DSBDC is temperature-independent. We suspect that this is caused by a competition of different mechanisms, which are also most-likely only weakly temperature dependent in the 300 K to 100 K range explored here.

The conductivity of the MOFs containing the three dopants is compared with the pure material in Fig. 4d. There is no significant difference between the conductivities. This suggests that the conductivity is more dominated by the linkers than by the metal nodes as these are unchanged between the materials. This allows us to tailor the catalytical properties of the metal centers without destroying the linker-enabled conductivity. The additional flexibility of this approach might not be limited to the DSBDC-MOF family and could have implications for other MOFs as well.

V. CONCLUSION

In this talk, we broaden the range of THz applications in material science to include the emerging field of metal-organic frameworks (MOFs). We utilized TDS to measure the ground state conductivity of Mn₂DSBDC at temperatures between 300 K and 100 K. Furthermore, we replaced manganese with nickel, cobalt, and copper and verified that the metals are successfully incorporated. The guest metals minutely changed the crystal structure and did not alter the conductivity.

The same THz techniques were also applied to another MOF, Zn₂TTFTB. In this MOF, we found an apparently pressure-dependent THz mode, which might be caused by guest molecules that can be expelled under static pressure. OPTP and TRTS of this MOF revealed a carrier lifetime spanning three orders of magnitude: sub-ps, 30 ps, and ns range. Our TRTS results fitted well to a Drude-Smith model, with a c parameter of - 0.86. A c-parameter close to -1 corresponds to a strongly suppressed particle to particle charge transfer, illustrating a core challenge for DC conductivity measurements on MOF powders, which is overcome by utilizing contact-free THz spectroscopy.

VI. ACKNOWLEDGEMENTS

I would like to thank the conference organizers for all the hard work they put into this conference and for giving me the opportunity to present our research to this great community. This research would not have been possible without funding; hence, I graciously acknowledge financial support from the National Science Foundation (NSF) under grant no. CHE-1954453. This research used 6-BM of the National Synchrotron

Light Source II, a U.S. Department of Energy (DOE) Office of Science User Facility operated for the DOE Office of Science by Brookhaven National Laboratory under Contract DE-SC0012704.

REFERENCES

- [1] J. Neu, and C.A. Schmuttenmaer, "Tutorial: An Introduction to Terahertz Time Domain Spectroscopy (THz-TDS)", *Journal of Applied Physics*, vol. 124, pp. 231101, 2018.
- [2] M. van Exter, and D. Grischkowky, "Optical and Electronic Properties of Doped Silicon from 0.1 to 2 THz", *Applied Physics Letters*, vol. 56, pp 1694, 1990
- [3] D. Zhao, H. Hu, R. Haselsberger, R.A. Marcus, M.-E. Michel-Beyerle, Y.M. Lam, J.-X. Zhu, C. La-o-vorakiat, M.C. Beard, and E.E.M Chia, "Monitoring Electron-Phonon Interactions in Lead Halide Perovskites Using Time-Resolved THz Spectroscopy", *ACS Nano*, vol. 13, pp. 8826, 2019.
- [4] M. D. Capobianco, B. Pattengale, J. Neu, and C.A. Schmuttenmaer, "Single Copper Atoms Enhance Photoconductivity in g-C₃N₄", *Journal of Physical Chemistry Letters*, vol. 11, pp. 8873-8879, 2020.
- [5] H. Li, M. Eddaoudi, M. O'Keeffe, and O. M. Yaghi, "Design and Synthesis of an Exceptionally Stable and Highly Porous Metal-Organic Framework", *Nature*, vol. 402, pp. 276, 1999.
- [6] B. Pattengale, J. Neu, A. Tada, G. Hu, C.J. Karpovich, and G.W. Brudvig, "Cation-exchanged Conductive Mn₂DSBDC Metal-Organic Frameworks: Synthesis, Structure, and THz Conductivity", *Polyhedron*, vol. 203, pp. 115182, 2021.
- [7] B. Pattengale, J. Neu, S. Ostresh, G, Hu, J.A. Spies, R. Okabe, G.W. Brudvig, and C.A. Schmuttenmaer, "Metal-Organic Framework Photoconductivity via Time-Resolved Terahertz Spectroscopy", *Journal of the American Chemical Society*, vol. 141, pp. 9793-979, 2019.
- [8] L. Sun, T. Miyakai, S. Seki, M. Dincă, "Mn₂(2,5-disulfhydrylbenzene-1,4-dicarboxylate): A Microporous Metal–organic Framework with Infinite (−Mn–S−)∞ Chains and High Intrinsic Charge Mobility", *Journal of the American Chemical Society*, vol. 135, pp. 8185-8188, 2013.
- [9] T. C. Narayan, T. Miyakai, S. Seki, M. Dincă, "High Charge Mobility in a Tetrathiafulvalene-Based Microporous Metal-Organic Framework", *Journal of the American Chemical Society*, vol. 134, pp. 12932, 2012.
- [10] L. Sun, C. H. Hendon, M. A. Minier, A. Walsh, and M. Dincă, "Million-Fold Electrical Conductivity Enhancement in Fe₂(DEBDC) versus $Mn_2(DEBDC)$ (E = S, O)", *Journal of the American Chemical Society*, vol. 137, pp. 6164, 2015.
- [11] J. Neu, K. Regan, J.R. Swierk, and C.A. Schmuttenmaer, "Applicability of the Thin-film Approximation in Terahertz Photoconductivity Measurements", *Applied Physics Letter*, vol. 113, pp. 233901, 2018.
- [12] C. La-o-vorakiat, L. Cheng, T. Salim, R. A. Marcus, M.-E. Michel-Beyerle, Y. M. Lam, and E. E. M. Chia, "Phonon Features in Terahertz Photoconductivity Spectra due to Data Analysis Artifact: A Case Study on Organometallic Halide Perovskites", *Applied Physics Letters*, vol. 110, pp 123901, 2017.
- [13] U. Tayvah, J.A. Spies, J. Neu, and C.A. Schmuttenmaer, "Nelly: A User-Friendly and Open-Source Implementation of Tree-Based Complex Refractive Index Analysis for Terahertz Spectroscopy", *Analytical Chemistry*, vol. 93, pp. 11243, 202.
- [14] R. Dong, P. Han, H. Arora, M. Ballabio, M. Karakus, Z. Zhang, C. Shekhar, P. Adler, P.S. Petkov, A. Erbe, S.C.B. Mannsfeld, C. Felser, T. Heine, M. Bonn, X. Feng, and E. Cánovas, "High-mobility Band-like Charge Transport in a Semiconducting Two-dimensional Metal-organic Framework", *Nature Materials*, vol. 17, pp. 1027-1032, 2018.
- [15] J. Neu, H. Nikonow, and C.A. Schmuttenmaer, "Terahertz Spectroscopy and Density Functional Theory Calculations of DL-Norleucine and DL-Methionine", *Journal of Physical Chemistry A*, vol. 122, pp. 5978, 2018.